Potassium isotope signatures in modern marine sediments:

2	Insights into early diagenesis
3	
4	Wenshuai Li ^{1,2} , Xiao-Ming Liu ^{1*} , Kun Wang ³ , James McManus ⁴ , Brian A. Haley ⁵ , Yoshio
5	Takahashi ² , Mohsen Shakouri ⁶ , and Yongfeng Hu ⁶
6	1. Department of Earth, Marine and Environmental Sciences, University of North
7	Carolina-Chapel Hill, NC, USA
8	2. Department of Earth and Planetary Science, Graduate School of Sciences,
9	University of Tokyo, Tokyo 113-0033, Japan
10	3. Department of Earth and Planetary Sciences and McDonnell Center for the Space
11	Sciences, Washington University in St. Louis, MO, USA
12	4. Bigelow Laboratory for Ocean Sciences, East Boothbay, ME, USA
13	5. College of Earth, Ocean, and Atmospheric Sciences, Oregon State University,
14	Corvallis, OR, USA
15	6. Canadian Light Source, University of Saskatchewan, Saskatoon, Canada
16	
17	Abstract: 323 words; Text: 6000 words
18	Figures: 6
19	Revision
20	Submitted to EPSL
21	
22	*Corresponding author, email: xiaomliu@unc.edu
23	
24	Keywords: MC-ICP-MS; XANES; Glauconite; Illite; Diagenesis; Authigenesis
25	
26	Abbreviations: MC-ICP-MS: Multicollector-Inductively Coupled Plasma Mass
~ ~	Consistence at a result of the Constitution of

Spectrometer; XANES: X-ray absorption near-edge structure; MAR: mass accumulation 27

rate; UCC: upper continental crust; PAAS: Post-Archean Australian Shale; OMZ: 28

oxygen-minimum zone 29

30

Abstract

31

32

33

34

35

36

37

38

39

40

41

42

43

44

45

46

47

48

49

50

51

52

53

54

The sedimentary fluxes controlling potassium (K) budget of the oceans and the isotope composition of K (δ^{41} K) potentially yield valuable information about the global K cycling. However, at present sedimentary diagenesis in the oceans is one of the least well-known components of the seawater K budget. This study presents a dataset of the modern (<50 cm) sediments from a range of hydrographic regimes including continental margin settings (the Peru Margin, California Borderland, and Mexican Margin) and deep-sea environments (the Equatorial Pacific). We determine the K isotope compositions and origins of K in the sediments and compare them with the results of elemental abundances and spectroscopic analyses. The wide variability in sedimentary K/Al and Rb/K ratios, Kphase distributions, and K isotope compositions support the interplay between continental weathering, which provides clastic inputs, and sedimentary diagenesis, which constitutes an important sink of seawater K. The net result of these processes potentially alters the K elemental and isotopic budgets in sediment strata of various marine environments. We demonstrate that K is dominantly hosted by illite, glauconite, and feldspars, and regional K-phase partitioning modulates marine sedimentary K budget. For example, considerable amounts of K hosted in illite (up to 90%) primarily of terrestrial origins increase Rb/K ratios, producing low δ⁴¹K in California Borderland sediments (-0.57 to -0.40‰), the Pescadero Slope from the Mexican Margin (-0.42 to -0.39%), and Equatorial Pacific deep-sea basins (-0.56 to -0.44%). In contrast, glauconite authigenesis causes decreases in the Rb/K ratio and relatively high δ^{41} K at a site along the Peru Margin (-0.35 to -0.29%), as well as at two other sites along the Mexican Margin (-0.39 to -0.27%). Despite the presence of

feldspar-K (<20%), δ^{41} K in the sediments reflects dominant contributions of detrital illite (δ^{41} K_{illite} ~ -0.56‰) and authigenic glauconite (δ^{41} K_{glauconite} ~ -0.18‰). We conclude that the formation of glauconite in the sediments takes up isotopically light K from seawater and serves as an important sink of seawater K (including K in seawater-derived porewater) (~1 to 16, average ~6 Tg K·yr⁻¹) during early diagenesis, especially on continental margins.

60

61

62

63

64

65

66

67

68

69

70

71

72

73

74

75

76

55

56

57

58

59

1. Introduction

Reverse weathering has been recognized as a key factor in stabilizing ocean-atmosphere carbon reservoirs (Mackenzie and Garrels, 1966; Michalopoulos and Aller, 1995; Holland, 2005). During reverse weathering, the formation of Al-silicate clays serves as one of the primary sinks of seawater silica, alkali metal (e.g., Li⁺ and K⁺) and alkali-earth metal (e.g., Ca²⁺ and Mg²⁺) ions. At the same time, reverse weathering releases CO₂ into the ocean and atmosphere, modulating seawater chemistry and Earth's climate (e.g., Mackenzie and Garreis, 1966; Dunlea et al., 2017). Previous studies suggested that the seawater K budget is closely associated with clay authigenesis in marine systems, which is related to mineralogy, sedimentation rate, water chemistry and other factors controlling clay formation (Michalopoulos and Aller, 1995; Loucaides et al., 2010; Berner and Berner, 2012; Santiago Ramos et al., 2018; Aubineau et al., 2019; Banerjee et al., 2020; Hu et al., 2020). However, identifying and quantifying authigenic K-bearing clays in marine sediments are challenging due to the high background of detrital clays, which are difficult to distinguish from their authigenic counterparts based on elemental and mineralogical analyses only (Hu et al., 2020). Consequently, K output fluxes from seawater, as well as

seawater-derived pore fluids, into marine authigenic Al-silicates during reverse weathering remains poorly defined.

79

80

81

82

83

84

85

86

87

88

89

90

91

92

93

94

95

77

78

Stable K isotopes (41K and 39K) could potentially provide valuable insights into seawater K uptake during marine sedimentary clay authigenesis because of the isotopic fractionation driven by fluid-solid interactions (see reviews in Wang et al., 2021). The K isotope difference (~0.6%) between modern seawater and bulk silicate Earth (BSE) reflects an interplay between 1) K sources from high-temperature basalt alteration and continental weathering, and 2) K sinks from Al-silicate authigenesis in marine sediments and low-temperature oceanic crust alteration (Li W-Q. et al., 2016; Santiago Ramos et al., 2018; Santiago Ramos et al., 2020; Hille et al., 2019; Li S. et al., 2019; Chen et al., 2020; Hu et al., 2020; Teng et al., 2020; Wang et al., 2020; Liu et al., 2021; Li W-S. et al., 2021a). Overall, marine sediments consume seawater K nearly two times the rate of lowtemperature oceanic crust alteration (K added into secondary clays), thus causing isotopic variations (Δ^{41} K_{sea-sed}) of ~0.4 to 0.6‰, as assessed in isotopic mass balance box models (Li S. et al., 2019; Hu et al., 2020). Santiago Ramos et al. (2018) investigated deep-sea sediments and suggested Δ^{41} K_{sea-sed} of ~0% (equilibrium clay K uptake) or ~0.5 to 2‰ (K⁺ desolvation). Based on a survey of global marine sediments, Hu et al. (2020) reported a wide range of Δ^{41} K_{sea-sed} (0.34 to 1.4%).

96

97

98

99

Clearly, there is a range of existing estimates from field observations (Hu et al., 2020) and predictions based on isotopic mass balance models (Li S et al., 2019; Hu et al., 2020) and one-D diffusion-advection-reaction models (Santiago Ramos et al., 2018). Such wide

ranges are not surprising, and the most likely causes include 1) there are different isotopic effects associated with clay formation in the oceans; 2) the source of K in sediments may have variable K isotope compositions, and 3) K isotope analyses were performed on bulk sediments (mostly multiminerallic) with compositional variations. Specifically, Santiago Ramos et al. (2018) inferred that δ^{41} K of marine sediments may be complicated by ionic diffusion, exchange, and clay formation. Hu et al. (2020) noted that δ^{41} K_{sed} can be partially overprinted by terrestrial materials and that the proportion of authigenic K in sediments is poorly quantified, which likely induces bias in the estimation of the isotopic fractionation between modern seawater K and K sequestrated in clays during sedimentary diagenesis $(\Delta^{41}K_{sea-sed})$. Santiago Ramos et al. (2018) suggested that authigenic and detrital phases in marine sediments and associated K isotope fractionation may vary depending on the nature of K hosts and characteristics of sedimentary settings (e.g., continental margins with high sedimentary fluxes vs. deep-sea basins with relatively low sedimentary fluxes). Therefore, further investigations on seawater K sequestration in clays and corresponding isotope fractionation during sedimentary diagenesis are needed.

115

116

117

118

119

120

121

100

101

102

103

104

105

106

107

108

109

110

111

112

113

114

In this study, we present the K phase distributions and isotope compositions of modern marine sediments from three continental margins (i.e., Peru Margin, California Borderland, and Mexican Margin) and three deep-sea (the Equatorial Pacific) sites. These data are used to address three basic questions related to K diagenesis in modern oceans: (i) What are the dominant sinks and sources of K in marine sediments and how do these vary as a function of depositional environments? (ii) Are there K isotope effects between fluid K

sources (seawater/pore-fluids) and secondary clays formed during marine sedimentary diagenesis? (iii) What is the role of marine clay authigenesis in the seawater K budget?

2. Field description

Our research areas vary in depositional regimes, from semi-restricted or open continental margins to deep-sea settings. Study sites include one site at the Peru Margin, three sites along the Mexican Margin, four submarine basins within the California Borderland region, and three deep-sea sites north of the equator towards Hawaii (Equatorial Pacific) (Fig. 1). At each site, modern marine sediments (< 50 cm depth) were sampled to evaluate early diagenesis. The continental margin samples were collected using a multiple corer several decades ago and the details of sampling and processing are presented elsewhere (e.g., Wheatcroft and Sommerfield, 2005; McManus et al., 2005). The Pacific sediments were collected in 2020 using an advanced piston corer and an extended core barrel during the cruise. Recovered cores with negligible sedimentary and sampling disturbance were subsampled immediately in the laboratory at 4°C on the ship.

The continental margin sites and associated samples have been reported previously (e.g., McManus et al., 2005; McManus et al., 2006; Poulson-Brucker et al., 2009; Little et al., 2016; Little et al., 2017; Bryan et al., 2021) and are therefore briefly introduced. The MC82 site is located at 264 m depth below the perennial Peru upwelling system and is featured by a moderate mass accumulation rate (25 mg·cm⁻²·yr⁻¹) (Böning et al., 2004, Table S1).

Studied sites along the Mexican Margin are the Soledad Basin, Pescadero Slope, and Magdelena Margin (Berelson et al., 2005). The Soledad and Magdalena sites are situated on the western side of Baja California at 692 and 544 m depth, respectively. The sediment accumulation rate at the Soledad site (50-90 mg·cm⁻²·yr⁻¹) is much higher than that of the Magdalena site (4–12 mg·cm⁻²·yr⁻¹) due to increased productivity and associated biogenic sedimentation (van Geen et al., 2003; Silverberg et al., 2004) (Table S1). The Pescadero Slope is situated at the eastern corner of the mouth of the Gulf of California (616 m depth) with high clastic inputs from continental drainage of the Sierra Madre Occidental Mountains (77 mg·cm⁻²·yr⁻¹) (Chong et al., 2012).

The sites at the California Borderland are the Santa Barbara Basin, the Santa Monica Basin, the Santa Catalina Basin, and the Tanner Basin. These sites are generally O₂ deficient due to restricted circulation of seawater and high primary production resulting from coastal upwelling (Macías et al., 2012). The Santa Barbara Basin and Santa Monica Basin are near-shore basins with water depths of 493 m and 905 m, respectively. The Santa Catalina Basin (1300 m) and Tanner Basin (1514m) are further off-shore. The mass accumulation rate in the Santa Barbara Basin is the highest among the studied sites (Table S1) due to the highest lithogenic flux in this area (Thunell et al., 1995).

Terrigenous sediments in studied Equatorial Pacific region are highly heterogeneous, with εNd ranging from ~ -10 (Asian dust) to +6 (volcanogenic sediments around Hawaii) (Nakai et al., 1993; Jones et al., 1994; Jones et al., 2000; Abbott et al., 2016). This study focuses on three distinct deep seafloor depositional settings: a red clay (Asian dust) site (Station

3), a carbonate-rich site (carbonate ooze, CaCO₃ ~14–65%, Station 4), and a siliceous site (radiolarian ooze, Station 5) (Isern, 1991; McManus et al., 1995; Murray et al., 2000) (Tables S1 and S7). The Equatorial Pacific sediments mostly reflect a mixture of red clay (dust), volcanic debris with diatomaceous silica and calcium carbonate contributions (Hammond et al., 1996). The essential point is that this transect represents a gradient of red clay and radiogenic island debris to biogenic-rich microfossil ooze. All sites are at ~4000 m (depth) or below, relatively low in organic carbon (core averages between 0.2 and 0.3%, supplementary data 2), and sedimentation rates are much lower compared with those of continental margin sites although not well defined. The Station 3 site represents slowly accumulating (~0.2 cm·ky⁻¹) red clay sediments (Isern, 1991). The Station 4 site becomes rich in carbonate (>50%) with some diatoms and radiolaria of 1 to 3 cm·ky⁻¹ (Isern, 1991; McManus et al., 1995; Murray et al., 2000). The Station 5 site is roughly at the termination of the equatorial carbonate ooze and has an accumulation rate of ~0.5 cm·ky⁻¹ (Isern, 1991; McManus et al., 1995; Murray et al., 2000). The accumulation rates are estimated from Pacific sites with published data and they are not based on direct observations for the specific sites.

183

184

185

186

187

188

189

167

168

169

170

171

172

173

174

175

176

177

178

179

180

181

182

3. Methodology

Details of the analytical methodologies and numerical data are provided in Supplementary Materials. In brief, the elemental compositions of samples and standards were measured using a Q-ICP-MS (Agilent 7900) at the University of North Carolina, Chapel Hill (Table S2). X-ray diffractogram (XRD) was measured using an X-ray powder diffractometer (Rigaku SmartLab) at Chapel Hill Analytical and Nanofabrication Laboratory (CHANL)

(Fig. S1). Chemical extraction of adsorbed K (exchangeable, NH₄Ac-K) and organically bound K (H₂O₂-K) in sediments was performed to estimate the proportion of "labile" K and potential impacts on K isotope compositions of the bulk sample. A sum of exchangeable and organic K represents the labile component. We note that the labile K component is procedurally defined (i.e., extracted using chemical reagents) and should thus be treated with caution in terms of the specific interpretation of that pool.

196

197

198

199

200

201

202

203

204

205

206

207

208

209

210

211

212

190

191

192

193

194

195

X-ray absorption spectra provide insights into the speciation of K present in the sediments (Li W-S.et al., 2020), and the distribution of K-bearing phases in the sediments was quantified using K K-edge X-ray absorption near-edge structure (XANES) spectra processed with linear combination fitting (LCF) at the Soft X-ray Micro-Characterization beamline at the Canadian Light Source (Fig. 2). Details of XANES-LCF analysis and processing are provided in the Supplementary Materials. The LCF analysis employed a combinatorial approach using Athena and the K standards used as fitting components were selected to reproduce the spectral features present. Possible references for XANES-LCF suggested by mineralogy (XRD in Fig. S1) include glauconite-K, celadonite-K, feldspar-K, smectite-K, muscovite-K, and illite-K (Fig. S4). We used the spectrum of Kfeldspar for analysis because K-feldspar rather than plagioclase should serve as the major feldspar-K host in the samples. In particular, celadonite and glauconite are known as important components of K-enriched "green clays" in the oceans (Nieto et al., 2021). It has been recognized that celadonite (KMg $_{0.8}$ Fe $^{2+}$ $_{0.2}$ Fe $^{3+}$ $_{0.9}$ Al0.1Si $_4$ O $_{10}$ (OH) $_2$, empirical formula, http://mindat.org/) is almost exclusively linked to erupted basic rocks in the deep oceans (Nieto et al., 2021). By contrast, glauconite (K_{0.6}Na_{0.05}Fe³⁺_{1.3}Mg_{0.4}Fe²⁺_{0.2}Al_{0.3}Si_{3.8}O₁₀(OH)₂, empirical formula, http://mindat.org/) commonly forms in siliciclastic and calcareous sediments of continental margin settings as a product of early diagenesis (Baldermann et al., 2015). In addition, a wide distribution of glauconite in continental margin sediments has been reported (e.g., Mullins and Rasch, 1985; Glenn and Arthur, 1988; Lund et al., 1992). Therefore, we used the spectrum of glauconite-K rather than celadonite-K for XANES analysis. The presence of glauconite in studied sediments was confirmed petrographically by optical observation (Fig. S2) and scanning electron microscopy (SEM) (Fig. S3).

Based on mineralogical information and spectral analysis, we determined illite, glauconite and feldspars to be the dominant K-bearing phases in studied sediments. While smectite is not found using XRD, possibly because its main peak (001) is out of the analyzed 20 range (Fig. S1), it is important to verify the absence of smectite, because Fe-smectite is considered to be an important K host in marine sediments and commonly inferred as a precursor of glauconite (Michalopoulos and Aller, 1995; Meunier and El Albani, 2007; Baldermann et al., 2013). Smectite-K was also not identified by XANES. This may be due to the general analytical error of XANES-LCF (~10%) or the detection limit of XANES (5 wt.%). Nonetheless, the presence of smectite-K cannot be precluded, and more sensitive detection methods are needed. It is possible that the smectite-K spectrum based on a Na-montmorillonite standard (SWy-2) cannot represent K in Fe-smectite interlayers in marine sediments. Again, we note that K hosts in addition to feldspars, illite and glauconite maybe be present and insights gained from XNAES-LCF may be limited by the fitting limitation and currently available standard spectra. Additional standard spectra may be

needed to provide greater insights into sedimentary K speciation. In sum, feldspars, illite, and glauconite are probably the dominate K-bearing phases in studied samples and other common K-bearing phases such as smectite is still possible but not detected in this study.

The K isotope analytical procedures are adapted from Chen et al. (2019), and the details of chromatography and isotope analysis of K are provided in Supplementary Materials. The K isotope compositions of sediments and standards were analyzed using an MC-ICP-MS at the Washington University in St. Louis (Table S4), and expressed in a delta notation (Table S3) (normalization to NIST SRM 3141a, Chen et al., 2019) by the following equation:

246
$$\delta^{41} \text{K (\%0)} = \left\{ \frac{(^{41} \text{K}/^{39} \text{K})_{\text{sample}}}{(^{41} \text{K}/^{39} \text{K})_{\text{NIST SRM 3141a}}} - 1 \right\} \times 1000, \tag{1}.$$

The reproducibility of K isotope analysis was confirmed using igneous rock standards BHVO-2 and GSP-2 (Table S5). Repeated measurements of certified references yielded a long-term (20 months) uncertainty of 0.11‰ (2 S.D., Chen et al., 2019) for K isotope analysis using MC-ICP-MS. We use a notation $\Delta^{41}K_{x-y}$ equal to $\delta^{41}K_x$ - $\delta^{41}K_y$ to express K isotope fractionation between the components x and y. The confidence intervals (95% c.i.) were used to reflect the analytical uncertainty:

253
$$95\% \text{ c. i. } (\%_0) = t_{n-1} \times \frac{S.D.}{\sqrt{n}}$$
 (2);

where S.D. represents the standard deviation over analytical sessions (n times), and t_{n-1} denotes the student t-factor with (n-1) degrees of freedom at a 95% confidence level.

4. Results

The elemental and isotopic characterization of K in marine sediments is provided in Table S3 and shown in Fig. 3.

4.1. K elemental concentrations

Overall, the K concentration (i.e., [K]) ranges from 6.8 to 29.7 mg/g and follows an order: Equatorial Pacific area ([K]_{ave} = 21.4 mg/g) > California Borderland ([K]_{ave} = 14.1 mg/g) > Mexican Margin ([K]_{ave} = 12.8 mg/g) > Peru Margin ([K]_{ave} = 7.5 mg/g). The Pescadero Slope and Station 5 sites (included in the calculation of average [K]) are exceptional cases, which have higher and lower [K] than others in the Mexican Margin and the Equatorial Pacific, respectively (Fig. 3a).

Direct comparison among K concentrations at different sites is confounded by the varying dilution effects of quartz, carbonates, and other K-depleted materials in the bulk samples, as revealed by XRD (Zhang et al., 2022). Hence, proper normalization is required, and the elemental ratios of K normalized to Al (Figs. 3b and 4) (i.e., Al is often considered to be predominantly detrital in its origin, Michalopoulos and Aller, 1995) are provided to estimate the relative abundance of K. There is a generally increasing pattern of the K/Al (mol/mol ×100) ratio: California Borderland (K/Alave = 22.1) < Equatorial Pacific area (K/Alave = 23.1) < Mexican Margin (K/Alave = 24.4) < Peru Margin (K/Alave = 26.3). We identified a gradual increase in the K to Al ratio from the Soledad Basin (K/Alave = 23.5) to the Pescadero Slope (K/Alave = 24.6) and to the Magdalena Margin (K/Alave = 25.5) in the Mexican Margin. The K/Al mass ratio at Station 3 (K/Alave = 23.4), Station 4 (K/Alave = 23.2) and Station 5 (K/Alave = 22.7) in the Equatorial Pacific are comparable. The intra-area

difference in K/Al is minor for the California Borderland. Extracted labile K (i.e., a sum of exchangeable K and organic K) ranges from 0.3 to 0.5 mg/g (Table S3), making up <5 wt.% of the total K pool in general.

4.2. K isotope compositions

The δ^{41} K values in these sediments (δ^{41} K_{sed}) range from -0.57 ± 0.06 to -0.27 ± 0.06‰ (95% c.i., n=7 to 8) (Table S3). Samples from different areas display different δ^{41} K values with increasing δ^{41} K similar to the pattern of the K/Al ratio (Figs. 3b-3c): Equatorial Pacific sites (δ^{41} K_{ave} = -0.51‰) and California Borderland Basins (δ^{41} K_{ave} = -0.46‰) < Mexican Margin (δ^{41} K_{ave} = -0.37‰) and Peru Margin (δ^{41} K_{ave} = -0.32‰). Along the Mexican Margin, the sediments from the Magdalena Margin exhibits higher δ^{41} K (δ^{41} K_{ave} = -0.30‰) relative to those of the Pescadero Slope (δ^{41} K_{ave} = -0.41‰) and Soledad Basin (δ^{41} K_{ave} = -0.38‰). The sediments in the Magdalena Margin have δ^{41} K comparable to that of the Peru Margin (δ^{41} K_{ave} = -0.32‰). In the California Borderland, the sediments in the Santa Barbara Basin exhibits lower δ^{41} K (δ^{41} K_{ave} = -0.55‰) relative to those of the Santa Monica Basin (δ^{41} K_{ave} = -0.47‰), Santa Catalina Basin (δ^{41} K_{ave} = -0.44‰) and Tanner Basin (δ^{41} K_{ave} = -0.44‰). However, intra-basin isotopic differences are close to or even smaller than the long-term analytical error (0.11‰, 2 S.D., Chen et al., 2019), so they should be interpreted with caution.

4.3. K-bearing phases

We have identified the three most likely K-bearing phases in the sediments, namely illite-K, glauconite-K, and feldspar-K (Fig. 2, detailed justification in Methodology), combined with mineralogical information (XRD) indicating the presence of glauconite (Figs. S1-S3). However, the quantification of XANES-LCF may be considered as conservative because LCF produces large analytical uncertainty in general (~10%) and other K-bearing phases (e.g., smectite-K) may not be identified because of the low abundance. Specifically, Illite-K makes up 32.4 to 92.8% K and is enriched in samples of the California Borderland (ave. 73.2% K) and the Equatorial Pacific area (ave. 89.2% K) compared with the Peru Margin (ave. 35.7% K) and the Mexican Margin (ave. 59.7% K). Glauconite-K is more enriched in samples of the Peru Margin (ave. 64.3% K) and the Mexican Margin (ave. 40.2% K) than the California Borderland (ave. 22.5% K) and the Equatorial Pacific (undetectable). This phase distribution of K in surface sediments agrees with previous observations of glauconite accumulation at some continental margin sites (Glenn and Arthur, 1988; Lund et al., 1992). Feldspar-K can only be identified in the Santa Barbara, Santa Monica and Santa Catalina basins (up to 10%) and the Equatorial Pacific area (7.2 to 14.3%).

5. Discussion

Our results indicate a $\delta^{41}K_{sed}$ variation of ~0.3‰ in these studied modern marine sediments (in the upper 50 cm depth) associated with the variation in major K-containing phases. Here, we determine the isotopic composition of K-phases and evaluate the relative contributions from continental weathering (K from clastic inputs) and sedimentary diagenesis (K from seawater and seawater-derived porewater) on the K pool and its isotope composition in modern marine sediments. Last, we provide broader implications with the first-order estimate for seawater K scavenging during early diagenesis.

5.1. K sources and processes

327

328

329

330

331

332

333

334

335

336

337

338

339

340

341

342

343

344

345

346

347

348

349

equilibrium to near-equilibrium.

Comprehensive geochemical and phase analysis allows us to decipher the main controls on δ^{41} K_{sed} variations (-0.57 to -0.27‰, Table S3) in modern marine sediments. In general, the metal isotope compositions in marine sediments often reflect mixing between surface interactions (e.g., sorption and dissolution) and elemental phase distributions of different isotopic compositions (e.g., Poulson-Brucker et al., 2009; Little et al., 2016; Little et al., 2017; Santiago Ramos et al., 2018; Bryan et al., 2021). Surface interactions may exert negligible impacts on δ^{41} K variations in our samples given two lines of evidence below. First, recent laboratory experiments confirmed that K isotope fractionation caused by clay adsorption is constant (~0.8%), and the adsorption process is limited in high-salinity environments due to Na⁺ replacement of K⁺ (Li W-S et al., 2021a). This process is likely the case in marine environments and is also supported by the measurements of labile K in the sediments studied here (<5 wt.% of the bulk K pool, Table S3). Despite adsorptiondriven K isotope fractionation of ~0.8% (Li W-S. et al., 2021a), the contribution of labile K on these sediments via adsorption-driven isotopic fractionation to the variation in δ^{41} K_{sed} would still be limited. Second, igneous rock dissolution experiments in closed systems confirmed that K isotope fractionation is negligible during silicate dissolution because of rapid isotopic equilibrium within hours (Li W-S. et al., 2021b). Although these sediments were situated in open systems, we infer that this dissolution-driven isotopic fractionation may also be negligible considering the long residence time of these sediments (years to millennia), which is likely long enough for fluid-solid systems evolving from far-fromDifferent contributions of K-bearing phases may generate isotopic variations in geological samples (Li W-S et al., 2022a; Li W-S et al., 2022b). Phase assessment from chemical extractions, mineralogy, and XANES indicates that K is dominantly hosted in illite, glauconite, and feldspars (Figs. S1-S3), with illite-K and glauconite-K making up more than 80% K in bulk sediments (Table S6). We estimate $\delta^{41}K_{glauconite}$ of ~ -0.18% and δ^{41} K_{illite} of ~ -0.56‰ using linear fitting (Figs. 5a and S3a). The endmember δ^{41} K values were estimated using those linear correlations listed in Fig. 5a (y=0.0035x-0.5310, R^2 =0.89) and Fig. S5a (y=0.0041x-0.1549, R^2 =0.85) with the x value (the fraction of the endmember) set to be 100%. The dominant contribution to the isotopic composition in studied sediments is from glauconite-K and illite-K (isotopically light relative to glauconite-K). Due to the small proportion of feldspar-K, its isotope composition cannot be easily determined (Fig. S5b). The important question to be resolved is the origin of illite-K and glauconite-K in marine sediments. Because illite is a common, K-rich detrital clay in terrestrial systems such as soil, dust, and loess deposits, it is likely that the illite-K phase present in marine sediments is partially sourced from weathering of fluvial and dust sourced materials. The authigenic origin of glauconite is supported by the isotopic fractionation between K hosted in glauconite (~ -0.18‰) and modern seawater (~0.12‰, Hille et al., 2019; Wang et al., 2020) is about 0.26% (Fig. 5a), revealing removal of isotopically light K from seawater during glauconite formation. Moreover, a positive correlation exists between Na/K and δ⁴¹K_{sed} (Fig. S6), consistent with the removal of K by glauconite (isotopically heavier than illite-K) from high Na/K fluids (e.g., brines and seawater). However, the presence of diagenetic illite in the sediments is possible. It is

351

352

353

354

355

356

357

358

359

360

361

362

363

364

365

366

367

368

369

370

371

difficult to distinguish clastic illite from diagenetic illite, and the links between K/AI (and Rb/K) with K phase distribution and δ^{41} K could provide further insights.

375

376

377

378

379

380

381

382

383

384

385

386

387

388

389

390

391

392

393

394

395

373

374

Clastic fluxes added into the California Borderland and the Equatorial Pacific basins are dominantly from rivers of southern California's Transverse Ranges and wind-blown Asian dust, respectively (Uematsu et al., 1983; Schwalbach and Gorsline, 1985; Warrick and Milliman, 2003). The K/Al molar ratios in marine sediments from the more off-shore basins (i.e., Santa Catalina and Tanner, K/Al of 22 to 24, K/Alave = 23, mol/mol ×100) are higher than those of near-shore basins (i.e., Santa Barbara and Santa Monic, K/Al of 20 to 21, K/Al_{ave} = 21, mol/mol ×100), and corresponding clastic sources (e.g., Transverse Ranges River sediments, K/AI = 19, mol/mol ×100; Napier et al., 2020). The K/AI difference implies a marked diagenetic imprint on off-shore sediments due to the supply of seawater with high K/Al ratios. The comparison between K/Al and δ^{41} K shows that diagenetic uptake of K (an increase in the K/Al ratio) can result in δ^{41} K_{sed} increasing towards a regressionestimated δ⁴¹K_{glauconite} value of -0.18‰ (Fig. 5a) of the Equatorial Pacific and California Borderland basins (glauconite-K poor) to the Peruvian and Mexican margins (glauconite-K rich) (Fig. 5b). Potassium in the Equatorial Pacific sediments largely reflects its clastic source given their K/Al (mol/mol ×100) ratios vary from ~22 to 24 (Table S3), similar to the Asian dust (the top of core LL44-GPC3, K/Al ~23–24, Kyte et al., 2001). Sediments of the Equatorial Pacific (dominantly supplied with the Asian dust, Uematsu et al., 1983) are featured by relatively low K/AI, low $\delta^{41}K_{sed}$ values (slightly higher than or similar to δ⁴¹K_{illite}) and high illite-K contents (>70%), indicating the predominance of illite of a detrital origin (Fig. 5b).

397

398

399

400

401

402

403

404

405

406

407

408

409

410

411

412

413

414

415

416

417

In addition to the K/AI (mol/mol ×100) proxy, the Rb/K ratio (mol/mol ×1000) may reflect the contribution of diagenetic uptake of K versus K inputs from terrestrial materials. This idea is built upon the notion that Rb⁺ is more efficiently retained by clays compared to K⁺ during continental weathering (Nesbitt et al., 1980; Hu et al., 2016), which produces high Rb/K in weathering residues (2.0, the Post Archean Australian Shale, PAAS, which are ancient, highly weathered terrestrial sources). In comparison, sedimentary diagenesis in the oceans could be linked to the addition of seawater with a low Rb/K (mol/mol ×1000) ratio ~0.7. In this study, Rb/K (mol/mol ×1000) ratios in Santa Barbara and Santa Monica sediments at the California Borderland are similar to that of the PAAS, implying that these sediments may have been subject to continental weathering before sedimentation (Fig. 4b). Supportively, near-shore basins display an elevated Rb/K ratio (2.3 to 2.5, ave. 2.4, mol/mol ×1000) relative to off-shore basins at the California Borderland (1.9 to 2.2, ave. 2.1, mol/mol ×1000). In addition, the Rb/K ratio in near-shore sediments is very close to that of the clastic sources (2.5, Transverse Ranges River sediments, Napier et al., 2020). Hence, near-shore (high Rb/K) rather than off-shore (low Rb/K) sediments reflec to strong clastic contribution (high Rb/K). The Rb/K ratio (1.4 to 1.7, mol/mol ×1000) in the Mexican Margin is lower than that of their clastic sources (~2.0, mol/mol ×1000; coastal deposits from the Gulf of California; Shumilin et al., 2002), indicating the impact of early diagenesis (Table S3). The Rb/K ratio of the Equatorial Pacific Sediments (1.9–2.1, mol/mol ×1000) is similar to that of Asian dust (2.0, mol/mol ×1000; the top of drilling core LL44-GPC3, Kyte et al., 2001), which suggests a negligible role of sedimentary diagenesis.

There is a negative correlation (R^2 =0.51) between the $\delta^{41}K_{sed}$ value and Rb/K ratio (Fig. 5c). On the one hand, this correlation usually indicates inputs from continental weathering, because sediment Rb/K ratios would increase due to preferential K solubilization during weathering; and lighter K is structurally incorporated into clays (mostly illite) while heavier K is released into waters (e.g., Li S et al., 2019; Chen et al., 2020; Teng et al., 2020; Wang et al., 2020). Therefore, continental weathering produces high Rb/K and low δ^{41} K to solid phases in fluvial suspended loads and sediments known as detrital inputs, which can be transported to continental margins. Supportively, the Santa Barbara Basin from the California Borderland receiving more detrital inputs exhibit lower δ^{41} K_{sed} and higher Rb/K and illite-K than other margin sites (Table S6). At the Mexican Margin, the Pescadero Slope impacted by detrital inputs exhibits lower δ⁴¹K_{sed} and higher Rb/K and illite-K compared to the Soledad Basin and the Magdalena Margin (Table S6). Nevertheless, detrital sediment addition linked to continental weathering alone may not explain the high $\delta^{41}K_{Sed}$ (up to -0.3‰), which is heavier than average terrestrial material (e.g., ave. δ^{41} K_{UCC} = -0.44±0.05‰, 2 S.D., n=88, Huang et al., 2020) (Fig. 5c).

434

435

436

437

438

439

440

441

419

420

421

422

423

424

425

426

427

428

429

430

431

432

433

On the other hand, we speculate that the observed Rb/K and $\delta^{41}K_{sed}$ correlation in Fig. 5c implies diagenetic K uptake. If so, reverse weathering should decrease Rb/K ratios (Hu et al., 2020) and generate high- $\delta^{41}K_{sed}$ values, as opposed to isotopically light illite-K. The Mexican (except for the Pescadero Slope receiving marked fluvial inputs, see field description) and Peru margins show the signature of diagenetic K uptake (i.e., lower Rb/K ratios than their clastic sources, Table S3). In addition, they have high $\delta^{41}K_{sed}$ values towards estimated $\delta^{41}K_{glauconite}$ (~ -0.18‰, Fig. 5a), corresponding to enriched glauconite-

K (up to ~68%). By contrast, sediments of the Equatorial Pacific sites (primarily supplied by Asian dust, Uematsu et al., 1983) are characterized by Rb/K ratios close to the Asian dust source (2.0, mol/mol ×1000; Kyte et al., 2001). And they show low $\delta^{41}K_{sed}$ values (slightly higher than or similar to $\delta^{41}K_{illite}$), consistent with high illite-K proportions (>70%), which supports the idea of detrital illite contributions. Therefore, the Rb/K ratio combined with $\delta^{41}K$ provides supportive evidence for a diagenetic origin of glauconite-K and a terrestrial origin of illite-K. Although a detrital origin of illite may still dominate our studied sediments, the presence of diagenetic illite cannot be excluded. Therefore, we infer that the estimated $\delta^{41}K_{illite} \sim$ -0.56% may reflect contributions from both detrital and diagenetic illite.

The data compilation of this study and Hu et al. (2020) are displayed in Fig. 5d, indicating there may be two directions of K isotope fractionation in marine sediments. Most data points fall into Region I, which potentially reflects an interplay between continental weathering and sedimentary diagenesis. This study reveals glauconite-K formation during early diagenesis modulating K isotope fractionation (Region I). Sediment samples from Ryukyu and the Antilles, however, exhibit low δ^{41} K values (-1.4 to -0.6‰) with a positive relationship between δ^{41} K_{sed} and Rb/K, and they fall in Region II (Hu et al., 2020, Fig. 5d). Possible diagenetic processes responsible for the relationship between δ^{41} K_{sed} and Rb/K in Region II were proposed by Hu et al. (2020), including (1) diagenetic smectite-to-illite transformation, and (2) clinoptilolite (a type of K-rich zeolite) authigenesis. Our sediment data are not located in Region II for two possible reasons. The first is that we do not have representative samples, despite a range of marine settings studied here. The second is

that shallow sediments may experience different diagenetic processes compared with their deeper counterparts.

467

468

469

470

471

472

473

474

475

476

477

478

479

480

481

482

483

484

485

486

465

466

5.2. Implications for oceanic K sequestration

A combination of phase and geochemical analyses supports the idea that glauconite is one of the major authigenic K-rich clays in continental margin sediments (see discussion in 5.1). In general, glauconite continues to take up K from seawater (or seawater-derived pore fluids) during early diagenesis (Baldermann et al., 2013; Baldermann et al., 2015; Baldermann et al., 2022). The absence of glauconite-K in deep-sea sediments (>2000 m) may be caused by limited supplies of Al and Fe (Meunier and El Albani, 2007; Baldermann et al., 2015). We emphasize that the Peru Margin has the highest fraction of glauconite-K (Table S6 and Fig. 2), in accord with the local enrichment of glauconite within the oxygen minimum zone (OMZ) (Glenn and Arthur, 1988; Suits and Arthur, 2000; Arning et al., 2009). Nevertheless, no consensus exists on the causes of glauconite enrichment in Peru margin sediments in the studied depth (within the OMZ). For example, Suits and Arthur (2000) suggested that the presence of glauconite was caused by the extensive release of Fe from nearby detritus and/or was partially derived from glauconite-bearing sediments directly below the OMZ, or by winnowing of bottom currents. In comparison, Arning et al. (2009) inferred that glauconite occurring within phosphorite crusts in the Peru OMZ was formed in-situ in ferruginous dysoxic (or weakly sulfidic) environments with an episodical presence of dissolved oxygen at the sediment-seawater interface that may be induced by rapidly changing hydrological energy regimes.

We suggest that the sequestration rate of K in glauconite (R) of each site at continental margins can be estimated based on the average values of bulk [K] and XANES-based glauconite-K proportion of marine sediments from each site (F_G), multiplied by the mass accumulation rate (MAR) of each site (Tables S1, S3 and S6, the equation R=[K] × F_G × MAR is shown in Fig. 6a). The sequestration rate of glauconite-K (R) positively correlates with the mass accumulation rate (MAR) according to the inter-area comparison (Fig. 6a), despite previous observations suggesting that rapid mass accumulation potentially inhibit glauconite formation (Baldermann et al., 2013; Baldermann et al., 2015). There is a wide range of K sequestration rates in glauconite (R) within the studied sites (Table S1): 0.028 mg K·cm⁻²·yr⁻¹ (Magdalena margin) < 0.044 mg K·cm⁻²·yr⁻¹ (Santa Monica Basin) ~ 0.046 mg K·cm⁻²·yr⁻¹ (Tanner basin and Santa Catalina Basin) < 0.122 mg K·cm⁻²·yr⁻¹ (Soledad Basin) < 0.286 mg K·cm⁻²·yr⁻¹ (Pescadero Slope) (Fig. 6a).

We admit that it is unclear to what extent the rates of glauconite-K sequestration reported can be generalized and transferable to other marine environments through space and time. Nonetheless, using the global continental margin area (defined as <2000 m depth, $S = \sim 37 \cdot 10^{12} \text{ m}^2$, Liu et al., 2000), we provide a first-order approximation of the present-day output flux of K associated with glauconite authigenesis (H) in the oceans using the low (or high) ends and the average of K sequestration rate in glauconite (R), multiplied by global continental margin area (S) (i.e., $H = R \times S$, shown in Fig. 6b). This calculation estimates that the average output flux of K sequestered by authigenic glauconite is $\sim 6 \text{ Tg}$ K·yr⁻¹, with a minimum value of $\sim 1 \text{ Tg K·yr}^{-1}$ and a maximum value of $\sim 16 \text{ Tg K·yr}^{-1}$ (Fig.

6b). Although calculated glauconite-K flux (H) has large uncertainties, our estimates are within the range of oceanic K output fluxes updated by Hu et al. (2020) (Fig. 6d) and in previous studies (e.g., Spivack and Staudigel, 1994; Elderfield and Schultz, 1996; Jarrard, 2003; Holland, 2005; Berner and Berner, 2012; Li S et al., 2019). Additionally, Baldermann et al. (2022) confirms the importance of glauconite formation at shallow shelf settings and provides a global estimate of 1.56 to 3.52 Tg K·yr⁻¹, using quantified glauconite content and average K content in glauconite grains in marine sediments. Their results agree well with our estimate using the glauconite-K proportion and the K concentration in bulk sediments. The outcomes demonstrate significant contributions of clay mineral authigenesis (particularly glauconite) to the marine K cycle.

Estimated K output fluxes ranging from ~1 to 16 Tg K·yr¹ during glauconite formation in the oceans, which accounts for ~2 to 44% K consumed by sedimentary diagenesis in the ocean (36-43.2 Tg K·yr¹, recently updated by Hu et al., 2020, Fig. 6b). The average glauconite-K flux (~6 Tg K·yr¹) is about half that of K consumed by present-day oceanic crust alteration at low-temperatures (12.4 to 19.2 Tg K·yr¹) (Hu et al., 2020) and the same order of magnitude as K sequestrated in authigenic Fe-illite in global mangrove forests (~0.8 to 3.1 Tg K·yr¹; Cuadros et al., 2016). Hence, estimated glauconite-K output fluxes agree with previous results of the key areas favoring clay authigenesis, such as mangrove forests, low-temperature hydrothermal sites, and continental margin deposits (Mackenzie and Garrels, 1966; Michalopoulos and Aller, 1995).

We suggest that our reported glauconite-K fluxes (Table S1) are conservative estimates because authigenic glauconite has been found only sporadically in coastal and deep-sea environments (e.g., Logvinenko, 1982; Giresse, and Wiewióra, 2001; Albani et al., 2005; Baldermann et al., 2015). The glauconite-K flux to deep-sea sediments is not considered in this study since glauconite-K in sampled Equatorial Pacific sediments cannot be detected (Table S6). Although further constraints from temporal investigations are still needed, we conclude that glauconite authigenesis significantly affects the oceanic K budget. In sum, the K isotope composition in modern marine sediments combined with elemental phase analysis emphasizes the importance of seawater K uptake by glauconite during early diagenesis.

6. Conclusions

- This study reports the K isotope composition in modern marine sediments and combines elemental and spectroscopic analyses to assess the major controls on δ^{41} K compositions. The results provide insights into constraining the present-day global K output flux during early diagenesis in marine sediments. Major conclusions are summarized as follows:
- 1) The modern marine sediments (<50 cm) collected from continental margins and deep-sea settings exhibit inter-area heterogeneity in solid K phase distribution (dominated by illite-K, glauconite-K, and feldspar-K) and its isotope composition (-0.57 to -0.27‰).
- 2) The δ^{41} K compositions in the sediments reflect an interplay between illite of detrital (major, derived from continental weathering) and diagenetic (minor) origins (~ -0.56‰), and the diagenetic fingerprint mainly strengthened by glauconite authigenesis (~ -0.18‰).

3) Our results support the idea that the combination of K isotope and XANES-based speciation analyses is useful to identify the origin of K in marine sediments and constrain oceanic K cycles. Estimated global glauconite-K flux is ~2-44% of the total K uptake by sedimentary diagenesis in the ocean, revealing its important role in balancing the marine K budget.

560

561

562

563

564

565

566

567

568

569

570

571

572

573

574

575

576

555

556

557

558

559

Acknowledgments

The authors acknowledge funding supports from the startup grant from the University of North Carolina, Chapel Hill to X.-M. Liu. We also acknowledge the funding support from the JSPS fellowship (No. P21313) to W. Li. Support to J. McManus was provided by NSF Grants 1850789 and 1657832. The XANES data were collected at the Canadian Light Source, with the approval of CLS proposal review committee (30G09959, 32GU010898, and 35S12446). The Canadian Light Source, a national research facility of the University of Saskatchewan, which is supported by the Canada Foundation for Innovation (CFI), the Natural Sciences and Engineering Research Council, the National Research Council, Canadian Institutes of Health Research, Government of Saskatchewan, and the University of Saskatchewan. This work was also supported by grants OCE 1850765 to B. Haley and OCE 1850789 to J. McManus. Continental margin samples were collected on various US NSF-funded cruises that were supported by several grants to J. McManus including NSF Grants OCE-021965, OCE-9911550, and OCE-9617929. We sincerely thank the captain David Martin and the entire crew for their guidance and help of Pacific sediment collection.

The following are the Supplementary data to this article: 579 Supplementary data 1. 580 This document contains detailed description of methodology, 6 figures (Figs. S1-S6) 581 and 7 tables (Tables S1-S7). They are quoted in the main text and used to support the 582 findings of the paper. 583 Supplementary data 2. 584 This document contains supportive data to build the figures in the main text and 585 supplementary data 1. 586 587 References 588 Abbott, A. N., Haley, B. A., McManus, J., 2016. The impact of sedimentary coatings on 589 590 the diagenetic Nd flux. Earth Planet. Sci. Lett. 449, 217-227. Albani, A., Meunier, A., Fürsich, F., 2005. Unusual occurrence of glauconite in a shallow 591 592 lagoonal environment (Lower Cretaceous, northern Aquitaine Basin, SW France). Terra Nova 17, 537-544. 593 594 Arning, E. T., Lückge, A., Breuer, L. C., Gussone, N., Birgel, D., Peckmann, J., 2009. Genesis of phosphorite crusts off Peru. Mar. Geol. 262, 68-81. 595 596 Aubineau, J., El Albani, A., Bekker, A., Somogyi, A., Bankole, O. M., Macchiarelli, R., Meunier, A., Riboullea, A., Reynaud, J. Y., Konhauser, K. O., 2019. Microbially 597 induced potassium enrichment in Paleoproterozoic shales and implications for 598 reverse weathering on early Earth. Nat. Comm. 10, 1-9. 599 Baldermann, A., Warr, L. N., Grathoff, G. H., Dietzel, M., 2013. The rate and 600 mechanism of deep-sea glauconite formation at the Ivory Coast-Ghana Marginal 601 Ridge. Clay Miner., 61, 258-276. 602 Baldermann, A., Warr, L. N., Letofsky-Papst, I., Mavromatis, V., 2015. Substantial iron 603 sequestration during green-clay authigenesis in modern deep-sea 604

Supplementary materials

578

605

sediments. Nat. Geosci. 8, 885-889.

- Baldermann, A., Banerjee, S., Czuppon, G., Dietzel, M., Farkaš, J., Löhr, S., Moser, U.,
- Scheiblhofer, E., Wright, N. M., Zack, T., 2022. Impact of green clay authigenesis
- on element sequestration in marine settings. Nat. Comm. 13, 1-11.
- Banerjee, S., Mondal, S., Chakraborty, P. P., Meena, S. S., 2015. Distinctive
- compositional characteristics and evolutionary trend of Precambrian glaucony:
- example from Bhalukona Formation, Chhattisgarh basin, India. Precambrian
- 612 Res. **271**, 33-48.
- Banerjee, S., Choudhury, T. R., Saraswati, P. K., Khanolkar, S., 2020. The formation of
- authigenic deposits during Paleogene warm climatic intervals: a review. J.
- Palaeogeogr. **9**, 1-27.
- Berelson, W. M., Prokopenko, M., Sansone, F. J., Graham, A. W., McManus, J. and
- Bernhard, J. M., 2005. Anaerobic diagenesis of silica and carbon in continental
- 618 margin sediments: discrete zones of TCO2 production. Geochim. Cosmochim.
- 619 Acta **69**, 4611-4629.
- Berner, E. K., Berner, R. A., 2012. Global environment: water, air, and geochemical
- 621 cycles. Princeton University Press.
- Böning, P., Fröllje, H., Beck, M., Schnetger, B., Brumsack, H. J., 2012. Underestimation
- of the authigenic fraction of Cu and Ni in organic-rich sediments. Mar. Geol., **323**,
- 624 24-28.
- Bryan, A. L., Dickson, A. J., Dowdall, F., Homoky, W. B., Porcelli, D., Henderson, G. M.,
- 2021. Controls on the cadmium isotope composition of modern marine
- sediments. Earth Planet. Sci. Lett. **565**, 116946.
- 628 Cuadros, J., Andrade, G., Ferreira, T. O., de Moya Partiti, C. S., Cohen, R., Vidal-
- Torrado, P., 2017. The mangrove reactor: Fast clay transformation and
- 630 potassium sink. Appl. Clay Sci. **140**, 50-58.
- 631 Chen, H., Tian, Z., Tuller-Ross, B., Korotev, R. L., Wang, K., 2019. High-precision
- potassium isotopic analysis by MC-ICP-MS: An inter-laboratory comparison and
- refined K atomic weight. J. Anal. At. Spectrom. **34**, 160-171.
- 634 Chen, H., Liu, X. M., Wang, K., 2020. Potassium isotope fractionation during chemical
- weathering of basalts. Earth Planet. Sci. Lett. **539**, 116192.

- 636 Chong, L. S., Prokopenko, M. G., Berelson, W. M., Townsend-Small, A. and McManus,
- J., 2012. Nitrogen cycling within suboxic and anoxic sediments from the
- continental margin of Western North America. Mar. Chem. **128**, 13-25.
- Dunlea, A. G., Murray, R. W., Ramos, D. P. S., Higgins, J. A., 2017. Cenozoic global
- cooling and increased seawater Mg/Ca via reduced reverse weathering. Nat.
- 641 Comm. **8**, 1-7
- Elderfield, H., Schultz, A., 1996. Mid-ocean ridge hydrothermal fluxes and the chemical
- composition of the ocean. Annu. Rev. Earth Planet. Sci. **24**, 191-224.
- 644 Giresse, P., Wiewióra, A., 2001. Stratigraphic condensed deposition and diagenetic
- evolution of green clay minerals in deep water sediments on the Ivory Coast—
- 646 Ghana Ridge. Mar. Geol. **179**, 51-70.
- 647 Glenn, C. R., Arthur, M. A., 1988. Petrology and major element geochemistry of Peru
- margin phosphorites and associated diagenetic minerals: authigenesis in modern
- organic-rich sediments. Mar. Geol. 80, 231-267.
- Hammond, D. E., McManus, J., Berelson, W. M., Kilgore, T. E., Pope, R. H., 1996. Early
- diagenesis of organic material in equatorial Pacific sediments: stpichiometry and
- kinetics. Deep-Sea Res. II: Top. Stud. Oceanogr. 43, 1365-1412.
- Hille, M., Hu, Y., Huang, T. Y., Teng, F. Z., 2019. Homogeneous and heavy potassium
- isotopic composition of global oceans. Sci. Bull., **64**, 1740-1742.
- Holland, H. D., 2005. Sea level, sediments and the composition of seawater. Am. J.
- 656 Sci. **305**, 220-239.
- Hu, Y., Teng, F. Z., Plank, T., Chauvel, C., 2020. Potassium isotopic heterogeneity in
- subducting oceanic plates. Sci. Adv. **6**, eabb2472.
- Hu, D., Clift, P. D., Wan, S., Böning, P., Hannigan, R., Hillier, S., Blusztajn, J., 2016.
- Testing chemical weathering proxies in Miocene–Recent fluvial-derived
- sediments in the South China Sea. Geol. Soc. Spec. Publ. **429**, 45-72.
- 662 Huang, T. Y., Teng, F. Z., Rudnick, R. L., Chen, X. Y., Hu, Y., Liu, Y. S., Wu, F. Y.,
- 663 2020. Heterogeneous potassium isotopic composition of the upper continental
- crust. Geochim. Cosmochim. Acta **278**, 122-136.
- lsern, A. R., 1991. Calcium carbonate and organic carbon accumulation in the central
- equatorial Pacific (Doctoral dissertation, University of Rhode Island).

- Jarrard, R. D., 2003. Subduction fluxes of water, carbon dioxide, chlorine, and potassium. Geochem. Geophys. Geosys. 4, 8905.
- Jones, C. E., Halliday, A. N., Rea, D. K., Owen, R. M., 1994. Neodymium isotopic
- variations in North Pacific modern silicate sediment and the insignificance of
- detrital REE contributions to seawater. Earth Planet. Sci. Lett. **127**, 55-66.
- Jones, C. E., Halliday, A. N., Rea, D. K., Owen, R. M., 2000. Eolian inputs of lead to the
- North Pacific. Geochim. Cosmochim. Acta **64**, 1405-1416.
- Kyte, F. T., Leinen, M., Heath, G. R., Zhou, L., 1993. Cenozoic sedimentation history of
- the central North Pacific: Inferences from the elemental geochemistry of core
- 676 LL44-GPC3. Geochim. Cosmochim. Acta **57**, 1719-1740.
- 677 Li, S., Li, W., Beard, B. L., Raymo, M. E., Wang, X., Chen, Y., Chen, J., 2019. K
- isotopes as a tracer for continental weathering and geological K cycling. Proc.
- 679 Natl. Acad. Sci. U. S. A. **116**, 8740-8745.
- Li, W., Beard, B. L., Li, S., 2016. Precise measurement of stable potassium isotope
- ratios using a single focusing collision cell multi-collector ICP-MS. J. Anal. At.
- Spectrom. **31**, 1023-1029.
- 683 Li, W., Liu, X. M., Hu, Y., 2020. Potassium and calcium K-Edge XANES in chemical
- compounds and minerals: Implications for geological phase
- identification. Geostand. Geoanal. Res. 44, 805-819.
- Li, W., Liu, X. M., Hu, Y., Teng, F. Z., Hu, Y., 2021a. Potassium isotopic fractionation
- during clay adsorption. Geochim. Cosmochim. Acta **304**, 160-177.
- 688 Li, W., Liu, X. M., Wang, K., Koefoed, P., 2021b. Lithium and potassium isotope
- fractionation during silicate rock dissolution: An experimental approach. Chem.
- 690 Geol. **568**, 120142.
- Li, W., Liu, X. M., Wang, K., Hu, Y., Suzuki, A., Yoshimura, T., 2022. Potassium
- incorporation and isotope fractionation in cultured scleractinian corals. Earth
- 693 Planet. Sci. Lett. **581**, 117393.
- 694 Li, W., Liu, X. M., Wang, K., Takahashi, Y., Hu, Y., Chadwick, O. A., 2022b. Soil
- 695 potassium isotope composition during four million years of ecosystem
- development in Hawai 'i. Geochim. Cosmochim. Acta **332**, 57-77.

- Little, S. H., Vance, D., McManus, J. Severmann, S., 2016. Key role of continental
- 698 margin sediments in the oceanic mass balance of Zn and Zn
- isotopes. Geology **44**, 207-210.
- Little, S. H., Vance, D., McManus, J., Severmann, S., Lyons, T. W., 2017. Copper
- isotope signatures in modern marine sediments. Geochim. Cosmochim.
- 702 Acta **212**, 253-273.
- Liu, H., Xue, Y. Y., Zhang, G., Sun, W. D., Tian, Z., Tuller-Ross, B., Wang, K., 2021.
- Potassium isotopic composition of low-temperature altered oceanic crust and its
- impact on the global K cycle. Geochim. Cosmochim. Acta **311**, 59-73.
- Liu, K. K., Iseki, K., Chao, S.Y., 2000. Continental margin carbon fluxes, in The
- Changing Ocean Carbon Cycle, edited by R. B. Hanson, H.W Ducklow and J. G.
- Field, pp. 187-239, Cambridge University Press, Cambridge.
- Loucaides, S., Michalopoulos, P., Presti, M., Koning, E., Behrends, T., Van Cappellen,
- 710 P., 2010. Seawater-mediated interactions between diatomaceous silica and
- terrigenous sediments: results from long-term incubation experiments. Chem.
- 712 Geol. **270**, 68-79.
- Logvinenko, N. V., 1982. Origin of glauconite in the recent bottom sediments of the
- ocean. Sed. Geol. **31**, 43-48.
- Lund, S. P., Gorsline, D. S., Henyey, T. L., 1992. Rock magnetic characteristics of
- surficial marine sediments from the California continental borderland. Earth
- 717 Planet. Sci. Lett. 108, 93-107.
- Mackenzie, F. T., Garrels, R. M., 1966. Chemical mass balance between rivers and
- oceans. Am. J. Sci. **26**, 507-525.
- McManus, J., Hammond, D. E., Berelson, W. M., Kilgore, T. E., Demaster, D. J.,
- Ragueneau, O. G., Collier, R. W., 1995. Early diagenesis of biogenic opal:
- Dissolution rates, kinetics, and paleoceanographic implications. Deep Sea Res.
- 723 Part II Top. Stud. Oceanogr. **42**, 871-903.
- McManus, J., Berelson, W. M., Klinkhammer, G. P., Hammond, D. E., Holm, C., 2005.
- Authigenic uranium: relationship to oxygen penetration depth and organic carbon
- rain. Geochim. Cosmochim. Acta **69**, 95-108.

- McManus, J., Berelson, W. M., Severmann, S., Poulson, R. L., Hammond, D. E.,
- Klinkhammer, G. P., Holm, C., 2006. Molybdenum and uranium geochemistry in
- continental margin sediments: paleoproxy potential. Geochim. Cosmochim.
- 730 Acta **70**, 4643-4662.
- Meunier, A., El Albani, A., 2007. The glauconite-Fe-illite-Fe-smectite problem: a critical
- review. Terra Nova **19**, 95-104.
- Michalopoulos, P., Aller, R. C., 1995. Rapid clay mineral formation in Amazon delta
- sediments: reverse weathering and oceanic elemental cycles. Science **270**, 614-
- 735 617.
- Mullins, H. T., Rasch, R. F., 1985. Sea-floor phosphorites along the Central California
- continental margin. Econ. Geol., 80, 696-715.
- Murray, R. W., Knowlton, C., Leinen, M., Mix, A. C., Polsky, C. H., 2000. Export
- production and carbonate dissolution in the central equatorial Pacific Ocean over
- the past 1 Myr. Paleoceanography **15**, 570-592.
- Nakai, S. I., Halliday, A. N., Rea, D. K., 1993. Provenance of dust in the Pacific
- 742 Ocean. Earth Planet. Sci. Lett. **119**, 143-157.
- Napier, T. J., Hendy, I. L., Fahnestock, M. F., Bryce, J. G., 2020. Provenance of detrital
- sediments in Santa Barbara Basin, California, USA: Changes in source
- contributions between the Last Glacial Maximum and Holocene. Geol. Soc. Am.
- 746 Bull. **132**, 65-84.
- Nesbitt, H. W., Markovics, G., 1980. Chemical processes affecting alkalis and alkaline
- earths during continental weathering. Geochim. Cosmochim. Acta **44**, 1659-
- 749 1666.
- Nieto, F., Abad, I., Bauluz, B., Reolid, M., 2021. Textural and genetic relationships
- between glauconite and celadonite at the nanoscale: two different structural-
- compositional fields. Eur. J. Miner. **33**, 503-517.
- Poulson-Brucker, R. L., McManus, J., Severmann, S., Berelson, W. M., 2009.
- Molybdenum behavior during early diagenesis: Insights from Mo
- isotopes. Geochem., Geophys. Geosys. **10**. Q06010.
- Romans, B. W., Normark, W. R., McGann, M. M., Covault, J. A., Graham, S. A., 2009.
- Coarse-grained sediment delivery and distribution in the Holocene Santa Monica

- Basin, California: implications for evaluating source-to-sink flux at millennial time scales. Geol. Soc. Am. Bull. **121**, 1394-1408.
- Rudnick, R. L., Gao, S., Holland, H. D., Turekian, K. K., 2003. Composition of the continental crust. The crust **3**, 1-64.
- Santiago Ramos, D. P., Morgan, L. E., Lloyd, N. S., Higgins, J. A., 2018. Reverse weathering in marine sediments and the geochemical cycle of potassium in seawater: Insights from the K isotopic composition (41K/39K) of deep-sea pore-fluids. Geochim. Cosmochim. Acta **236**, 99-120.
- Santiago Ramos, D. P., Coogan, L. A., Murphy, J. G., Higgins, J. A., 2020. Lowtemperature oceanic crust alteration and the isotopic budgets of potassium and magnesium in seawater. Earth Planet. Sci. Lett. **541**, 116290.
- Schwalbach, J. R., Gorsline, D. S., 1985. Holocene sediment budgets for the basins of the California continental borderland. J. Sed. Res. **55**, 829-842.
- Shumilin, E. N., Carriquiry, J. D., Camacho-Ibar, V. F., Sapozhnikov, D., Kalmykov, S.,
 Sánchez, A., Aguíñiga-García, S., Sapozhnikov, Y. A., 2002. Spatial and vertical
 distributions of elements in sediments of the Colorado River delta and Upper Gulf
 of California. Mar. Chem. 79, 113-131.
- Silverberg, N., Martínez, A., Aguíñiga, S., Carriquiry, J. D., Romero, N., Shumilin, E.,
 Cota, S., 2004. Contrasts in sedimentation flux below the southern California
 Current in late 1996 and during the El Niño event of 1997–1998. Estuar. Coast.
 Shelf Sci. 59, 575-587.
- Spivack, A. J., Staudigel, H., 1994. Low-temperature alteration of the upper oceanic crust and the alkalinity budget of seawater. Chem. Geol. **115**, 239-247.
- Suits, N. S., Arthur, M. A., 2000. Sulfur diagenesis and partitioning in Holocene Peru shelf and upper slope sediments. Chem. Geol. **163**, 219-234.
- Teng, F. Z., Hu, Y., Ma, J. L., Wei, G. J., Rudnick, R. L., 2020. Potassium isotope
 fractionation during continental weathering and implications for global K isotopic
 balance. Geochim. Cosmochim. Acta 278, 261-271.
- Thunell, R. C., Tappa, E., Anderson, D. M., 1995. Sediment fluxes and varve formation in Santa Barbara Basin, offshore California. Geology **23**, 1083-1086.

788	Uematsu, M., Duce, R. A., Prospero, J. M., Chen, L., Merrill, J. T., McDonald, R. L.,
789	1983. Transport of mineral aerosol from Asia over the North Pacific Ocean. J.
790	Geophys. Res. Oceans 88, 5343-5352.
791	Van Geen, A., Zheng, Y., Bernhard, J. M., Cannariato, K. G., Carriquiry, J., Dean, W.
792	E., Eakins, B. W., Ortiz, J. D., Pike, J., 2003. On the preservation of laminated
793	sediments along the western margin of North America. Paleoceanography 18.
794	1098
795	Wang, K., Close, H. G., Tuller-Ross, B., Chen, H., 2020. Global average potassium
796	isotope composition of modern seawater. ACS Earth Space Chem. 4, 1010-
797	1017.
798	Wang, K., Li, W., Li, S., Tian, Z., Koefoed, P., Zheng, X. Y., 2021. Geochemistry and
799	Cosmochemistry of potassium stable isotopes. Geochemistry 125786.
800	Warrick, J. A., Milliman, J. D., 2003. Hyperpycnal sediment discharge from semiarid
801	southern California rivers: Implications for coastal sediment budgets. Geology 31,
802	781-784.
803	Wheatcroft, R. A., Sommerfield, C. K., 2005. River sediment flux and shelf sediment
804	accumulation rates on the Pacific Northwest margin. Cont. Shelf Res., 25, 311-
805	332.
806	Zeng, H., Rozsa, V. F., Nie, N. X., Zhang, Z., Pham, T. A., Galli, G., Dauphas, N., 2019.
807	Ab initio calculation of equilibrium isotopic fractionations of potassium and
808	rubidium in minerals and water. ACS Earth Space Chem. 3, 2601-2612.
809 810 811	Zhang, X. Y., Gaillardet, J., Barrier, L., Bouchez, J., 2022. Li and Si isotopes reveal authigenic clay formation in a palaeo-delta. Earth Planet. Sci. Lett. 578 , 117339.
812	
813	
814	

Figures

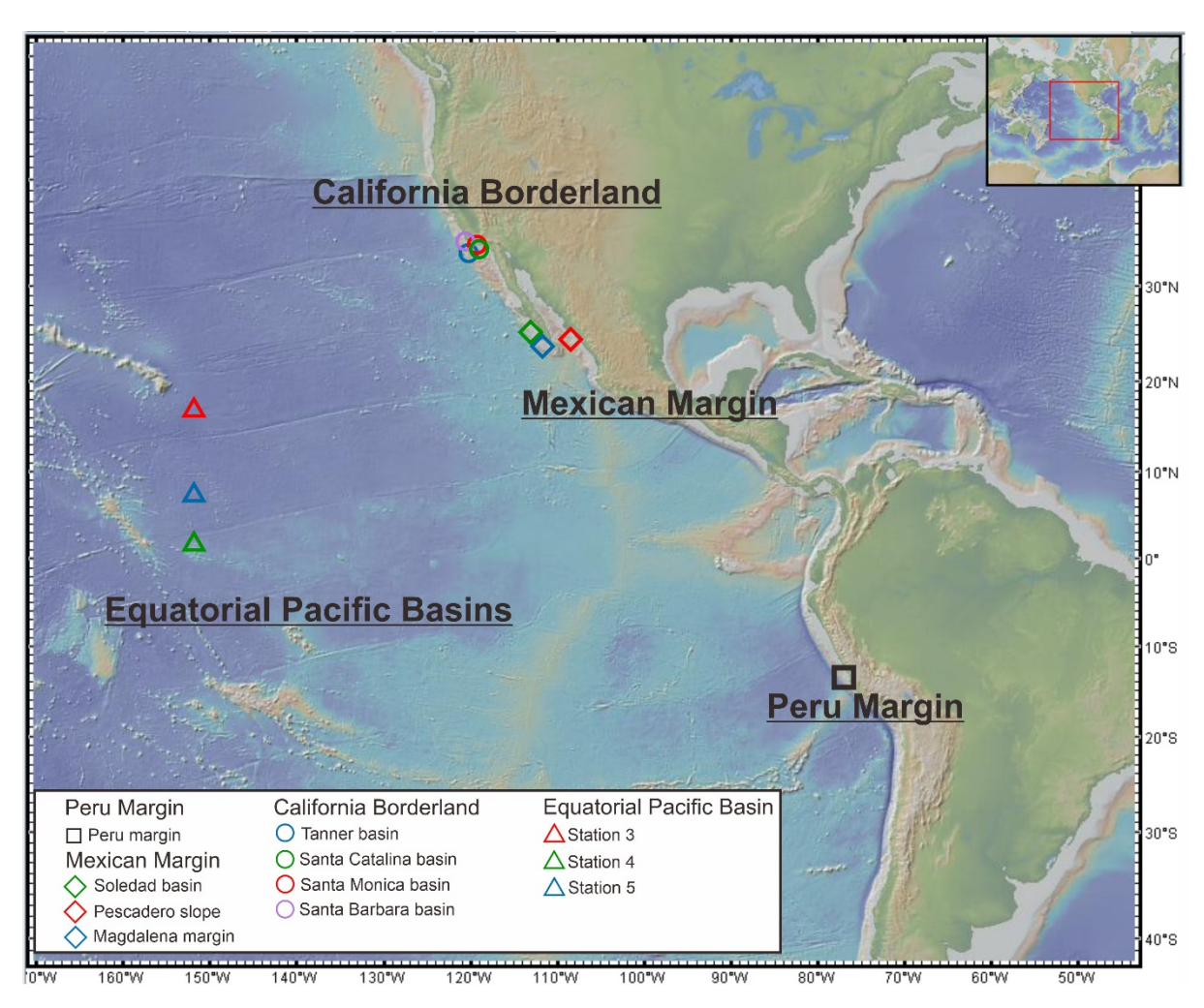


Fig. 1. Location of sampling sites included in this study. The Peru Margin is from the MC82 core of the Peruvian OMZ (McManus et al., 2006). The California Borderland Basins include: i) Tanner Basin, ii) Santa Catalina Basin, iii) Santa Monica Basin, and iv) Santa Barbara Basin. The Mexican Margin sites include: i) Soledad Basin, ii) Pescadero Slope, and iii) Magdalena Margin. Equatorial Pacific Basins include three sites north of the equator towards Hawaii (Station 3 to 5). Maps were made using GeoMapApp software (www.geomapapp.org).

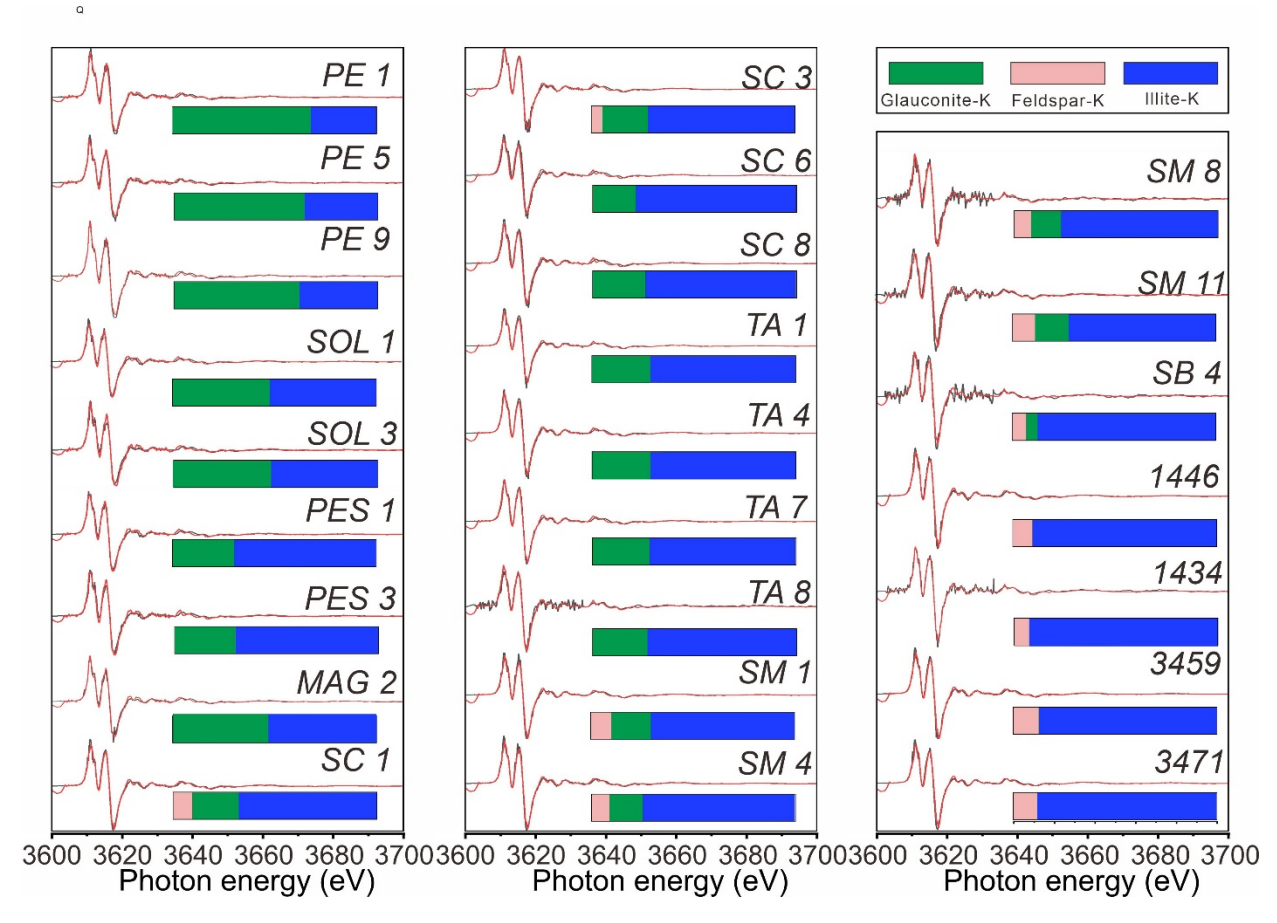


Fig. 2. K *K*-edge XANES-LCF spectra of studied samples using the first derivatives. Three major phases can be determined, including illite (blue), glauconite (green), and feldspar (pink). The raw data (black line) and LCF data (red line) are displayed. Note: PE 1, 5 and 9 are from the MC82 site of the Peru Margin; SOL 1 and 3 are from the Soledad Basin of the Mexican Margin; PES 1 and 3 are from the Pescadero Slope of the Mexican Margin; MAG 2 is from the Magdalena Margin of the Mexican Margin; SC 3, 6 and 8 are from the Santa Catalina Basin of the California Borderland; TA 1, 4, 7 and 8 are from the Tanner basin of the California Borderland; SM 1, 4, 8 and 11 are from the Santa Monica Basin of the California Borderland; SB 4 is from the Santa Barbara Basin of the California Borderland; 1446 and 1434 are from the Station 3 at the Equatorial Pacific Ocean; 3459 and 3471 are from Station 4 at the Equatorial Pacific Ocean. Detailed information of the sample number and location can be found in Table S3.

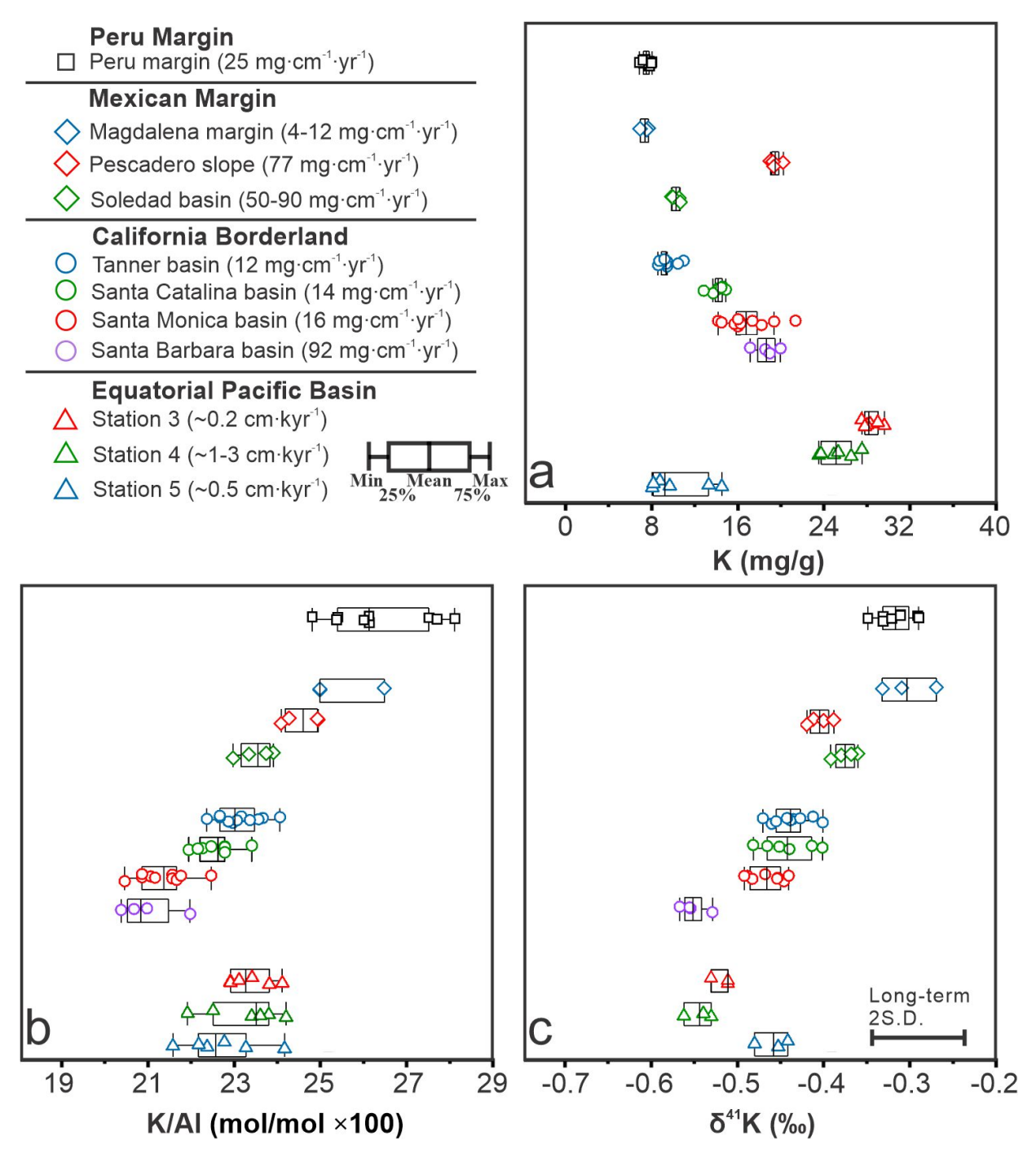


Fig. 3. Plots of measured K chemistry of smarine sediments, including (a) K concentration ([K]), (b) K/Al ratio, and (c) δ^{41} K_{sed} value (the long-term uncertainty of 0.11‰, Chen et al., 2019). Estimated sedimentation rates are provided in the legend of each region (see Field Description section and Table S1).

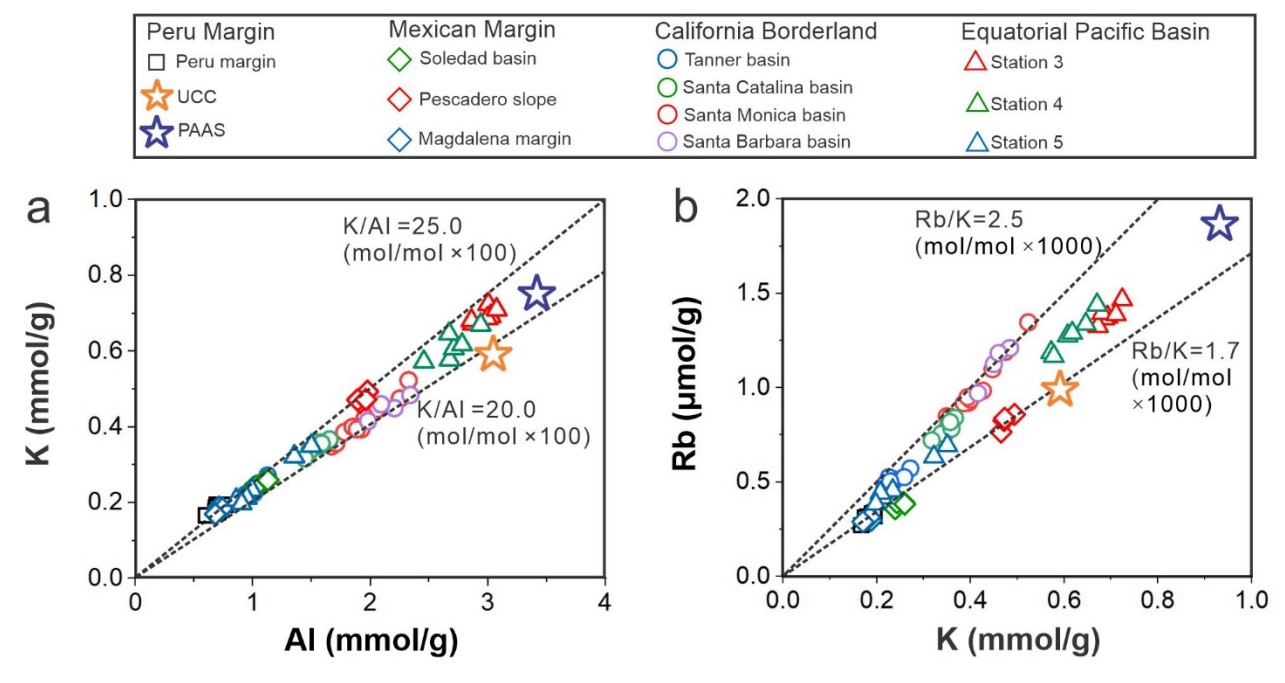


Fig. 4. Plots of bulk K concentration versus (a) Al and (b) Rb concentration. The element compositions of the Post Archean Australian Shale (PAAS) and upper continental crust (UCC) are provided for comparison. We note that dashed lines are guiding lines showing different K/Al (or Rb/K) ranges, which help to constrain the variation in elemental ratios.

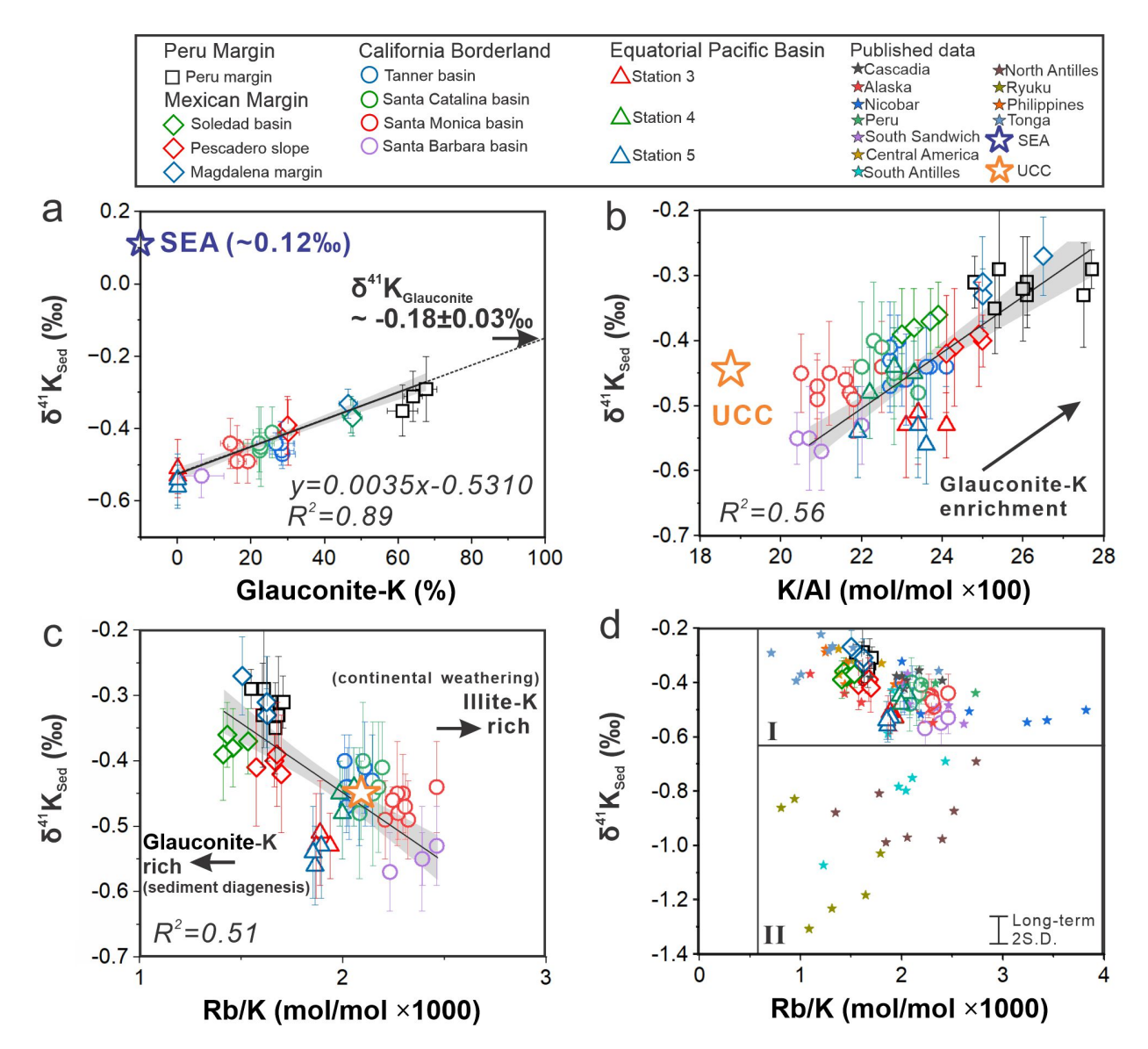


Fig. 5. Plots of (a) XANES-based glauconite-K versus δ^{41} K, (b) K/Al molar ratio versus δ^{41} K, (c) Rb/K molar ratio versus δ^{41} K in studied and published samples. Comparisons between Rb/K ratio and K isotope composition in marine sediments from (c) this study, and (d) a compilation of marine sediment data (this study and Hu et al., 2020). In plot (a), seawater K isotope composition (δ^{41} K_{sea}, Hille et al., 2019) is marked for comparison. In plots (b and c), UCC K isotope composition (δ^{41} K_{UCC}, Huang et al., 2020) is shown. In plot (d), regions I and II have distinct directions of K isotope fractionation as Rb/K ratio changes. Linear fittings are shown (black lines) and 95% confidence intervals are depicted (grey). A long-term 2 S.D. uncertainty of 0.11‰ is provided in Chen et al. (2019).

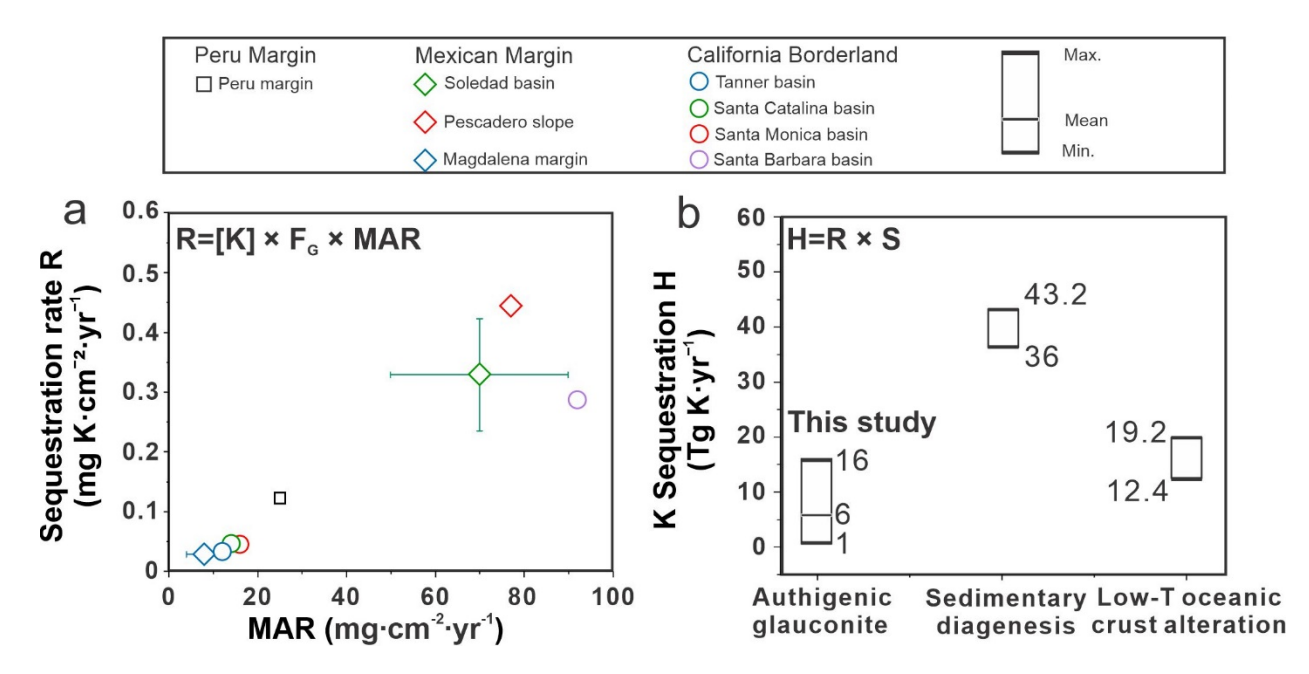


Fig. 6. Sequestration of K in glauconite during sedimentary diagenesis. (a) Sequestration rate in glauconite for studied continental margin sites ($R=[K] \times F_G \times MAR$). (b) Comparison between K sequestration fluxes of glauconite authigenesis ($H=R \times S$, see details in the text). The K sequestration fluxes of marine sedimentary diagenesis and oceanic crust alteration at low temperatures are from Hu et al. (2020).